Shaped Pupil Design for Future Space Telescopes

A J Eldorado Riggs[a], Neil Zimmerman[a], Alexis Carlotti[b], N. Jeremy Kasdin[a], Robert Vanderbei[a]

[a]Princeton University, Princeton, NJ USA
[b]Universite Joseph-Fourier, IPAG, 414 Rue de la Piscine, France

ABSTRACT

Several years ago at Princeton we invented a technique to optimize shaped pupil (SP) coronagraphs for any telescope aperture. In the last year, our colleagues at the Jet Propulsion Laboratory (JPL) invented a method to produce these non-freestanding mask designs on a substrate. These two advances allowed us to design SPs for two possible space telescopes for the direct imaging of exoplanets and disks, WFIRST-AFTA and Exo-C. In December 2013, the SP was selected along with the hybrid Lyot coronagraph for placement in the AFTA coronagraph instrument. Here we describe our designs and analysis of the SPs being manufactured and tested in the High Contrast Imaging Testbed at JPL. We also explore hybrid SP coronagraph designs for AFTA that would improve performance with minimal or no changes to the optical layout. These possibilities include utilizing a Lyot stop after the focal plane mask or applying large, static deformations to the deformable mirrors (nominally for wavefront correction) already in the system.

Keywords: AFTA, WFIRST, Shaped Pupil, Coronagraphy, Exoplanets, Deformable Mirror, High Contrast

1. INTRODUCTION

The direct imaging of exoplanets is a major technical challenge. The few exoplanets that have been directly imaged to date are massive, self-luminous, and at large angular separations from their host stars. To image cool exoplanets at small separations on the order of 100 milliarcseconds (mas), we require raw planet-to-star contrast ratios of 10^{-8} or better (referred to as high contrast). Even with perfect optics, the stellar PSF would overwhelm that of a dim companion, so several types of coronagraphs have been developed to suppress diffracted starlight. These coronagraphs must be on a space observatory because the atmosphere limits contrast on the ground to no better than 10^{-7} or 10^{-8}. NASA is currently studying two possible coronagraph-equipped space observatories, Exo-C and WFIRST-AFTA. In this paper we discuss the ongoing shaped pupil (SP) coronagraph development for WFIRST-AFTA at Princeton's High Contrast Imaging Laboratory and the Jet Propulsion Laboratory (JPL). First we cover the regular SP designs for AFTA, and in later sections we show designs for higher-performing coronagraphs that incorporate a SP with either a Lyot stop or large, static DM deformations. We also include a brief section on the submitted Exo-C SP design that was not selected.

2. 2-D OPTIMIZED SHAPED PUPIL DESIGN AND MANUFACTURE

Shaped pupils are theoretically the simplest type of coronagraph. They use a binary-transmission amplitude mask at a pupil plane to shape a star's point spread function (PSF) to have a region of high contrast, called the search area or discovery space. In practice, a focal plane mask (FPM) is also necessary to block the core of the stellar PSF. Unlike in a Lyot coronagraph, however, the FPM does not have a diffractive role and is instead used for better dynamic range on the detector. As long as the material for the SP is achromatic, the resulting PSF is also achromatic (but does scale in size with wavelength). The major performance parameters used to design the SP coronagraph are the inner working angle (IWA), outer working angle (OWA), contrast level, and azimuthal angular extent of the search area. The transmission of the mask is maximized subject to these constraints in a linear programming problem, as described in Carlotti et al.[1] and Vanderbei.[2] Other coronagraphs can sometimes achieve better contrast or IWA, but this gain comes with a higher sensitivity to misalignment and low-order aberrations.

Send correspondence to A.J. Riggs: ariggs@princeton.edu

Space Telescopes and Instrumentation 2014: Optical, Infrared, and Millimeter Wave, edited by Jacobus M. Oschmann, Jr., Mark Clampin, Giovanni G. Fazio, Howard A. MacEwen, Proc. of SPIE Vol. 9143, 914325 · © 2014 SPIE
CCC code: 0277-786X/14/$18 · doi: 10.1117/12.2056371

The main problem with 2-D optimized SPs has been their manufacturability. The 2-D optimizations produce disconnected obscurations, unlike the easily made, free-standing ripple SPs that JPL's Microdevices Lab (MDL) has manufactured over the past decade.[3,4] We must therefore lay these 2-D patterns on a substrate. We have considered transmissive masks of aluminum on glass manufactured in the same way as the microdot apodizer for the Gemini Planet Imager (GPI).[5,6] Preliminary analysis suggests that ghosting and chromaticity from the glass substrate would not work for a SP on AFTA because, unlike for GPI, we are working in the visible spectrum at higher contrast levels. Instead, the baseline design for AFTA and any other 2-D optimized SP is a reflective mask. Balasubramanian et al.[4] invented a way to make reflective SPs (RSPs) on silicon wafers. The wafer surface has black silicon regions to absorb light and aluminum regions for reflection. Several-millimeter thick, polished wafers are used to keep the surface height errors well within the range that a deformable mirror (DM) can correct. Specular reflectivity measurements and recent tests in JPL's High Contrast Imaging Testbed (HCIT) indicate that the black silicon is indeed black enough to achieve the high contrast required for WFIRST-AFTA. We should also note that SPs in reflection must be stretched along one axis to account for projection of the pupil. We have chosen to optimize our designs on a square grid and stretch the SP pixels for manufacturing only. This strategy allows for easier modeling on a computer, since a square grid with binary values can be used to model the SP in an unfolded optical layout.

For now we are still using free-standing FPMs made via Deep Reactive-Ion Etching (DRIE) of SOI wafers.[4] DRIE-made FPMs introduce no aberrations since they are through-hole masks. However, in order to implement SPs with 360° search areas we will have to lay the FPM designs on a substrate. Unlike at a pupil plane, however, an aluminum-on-glass FPM should be acceptable because the bright part of the stellar PSF will be blocked, so ghosting is less of an issue.

3. SHAPED PUPIL DESIGNS FOR AFTA

3.1 Specifics for AFTA

The WFIRST-AFTA space telescope would launch early in the next decade for a six year nominal mission. AFTA is a 2.4-meter telescope whose primary and secondary mirror structure was donated to NASA by the National Reconnaissance Office in 2012. With its wide field-of-view (over 200 times larger than Hubble's), AFTA will primarily be a survey telescope for the study of dark energy and microlensing. NASA plans to include a coronagraph instrument on AFTA for the direct imaging of tens of gas and ice giant exoplanets discovered beforehand from the ground by the radial-velocity technique. Up to a year of observing time will be dedicated to exoplanet imaging. Because AFTA was not specifically designed for the direct imaging of exoplanets, it does not have the pointing stability or pupil geometry necessary to image earth-like exoplanets. Nevertheless, the AFTA coronagraph will gather valuable new data on large, cool exoplanets and demonstrate the viability of high-contrast coronagraphs and deformable mirrors in space.

The AFTA telescope pupil requires a 2-D optimized SP (versus a 1-D optimized SP such as a concentric ring mask) to account for the secondary mirror and spider obstructions. Carlotti et al.[7] performed a thorough analysis of 2-D optimized SP designs for an AFTA-like telescope pupil, and our current designs follow from those results. The performance of a SP coronagraph with the actual AFTA pupil is slightly worse than in our previous analysis because the secondary mirror is off-axis, larger, and surrounded by several small obstructions (see Fig. 1(a)). Nevertheless, we follow the overall design procedure in Carlotti et al.[7] of having two classes of SPs: a discovery mask and a set of three characterization masks. The IWA of a 360° search area SP, i.e. a discovery mask, is too large ($> 5.5\lambda/D$, depending on the OWA) for follow-up spectral characterization of known nearby radial velocity planets. AFTA SPs with search areas of smaller angular extent, in this case 60° on opposite sides of the star, allow us to achieve an IWA of about $4\lambda/D$. The AFTA pupil has approximately a three-fold rotational symmetry, so with a set of three (nearly identical) masks rotated by 60° from each other we can cover the whole angular extent outside the IWA. Our proposed observing strategy for AFTA is thus to use the 360° mask for discovery of exoplanets in a blue bandpass since the PSF's IWA scales down with wavelength. For spectral characterization in redder light (from $600-950$ nanometers), we would then select the characterization mask whose search area aligned with the exoplanet. We would prefer the characterization SPs to have search areas greater than 60° across for stitching together disks and imaging exoplanets at the borders, but that would decrease performance in IWA or contrast. AFTA is currently planned to have two 48×48 actuator Xinetics

DMs, which limits the controllable region to $\pm 24\lambda/D$ vertically and horizontally in the image plane. Because of the large amounts of memory required to control over such a large region and the lack of radial velocity-detected exoplanets at large separations, the maximum desired OWA of the AFTA coronagraph may be reduced to somewhere in the range of 10 to $16\lambda/D$. A field stop is required to block the bright, uncontrolled parts of the stellar PSF, so the maximum desired OWA will need to be chosen well before launch.

SP optimization relies on symmetry in the pupil plane for greater speed and tractability. The Fourier transform is separable in Cartesian coordinates only (except for the special case of a circularly symmetric pupil). Each axis (x- or y-) of symmetry speeds up the optimization by reducing the number of constraints and points in the pupil and image planes. The AFTA pupil has approximately a three-fold rotational symmetry, but in Cartesian coordinates this means we can enforce just one axis of symmetry. To properly account for the slightly off-axis pupil and the small obstructions near the secondary mirror, we symmetrize the pupil about the y-axis as shown in Fig. 1 before running our optimizations. To clarify, symmetrizing the pupil can only lower the transmission because we copy any obstructed point on one half of the pupil to the other. For example, notice in the symmetrized pupil of Fig.1(b) how the circular obstructions increased from the number in Fig.1(a). Because the pupil is slightly off-axis for the coronagraph instrument, we effectively make the secondary mirror wider and the spiders thicker by symmetrizing. However, we do not believe symmetrization is significantly decreasing the performance of the SPs. We have verified for a few characterization masks that a full-pupil optimization of the asymmetric pupil yields essentially the same SP as a half-pupil optimization of the symmetrized pupil. It is apparently easiest for the SP optimizer to force symmetry on a nearly-symmetric pupil, so we have gone back to optimizing over just the symmetrized half pupil.

3.2 Alignment Tolerances and Pupil Padding

After manufacturability (which we already addressed), the next major concern is alignment of the SP to the actual pupil. A simple way to increase the SP's alignment tolerance is to pad the pupil obstructions with extra black pixels before running the SP optimization. However, the more we pad the starting pupil the worse the performance becomes–throughput decreases and IWA increases for fixed OWA and contrast level. (The obvious increase in IWA from the fact that the diameter of the telescope is shrinking turns out not to be the main cause of IWA degradation.) When padding by a pixel, a white (transmission=100%) pixel is converted to black (transmission=0%) if any of its eight neighbors are black. The symmetrized pupil in Fig. 1(b) still has anti-aliased (gray) pixels, and a padding of zero pixels means that we simply blacked out all the gray ($0\% <$ transmission $< 100\%$) pixels. An interesting property is that SPs optimized without any pupil padding end up maintaining the anti-aliased edges.

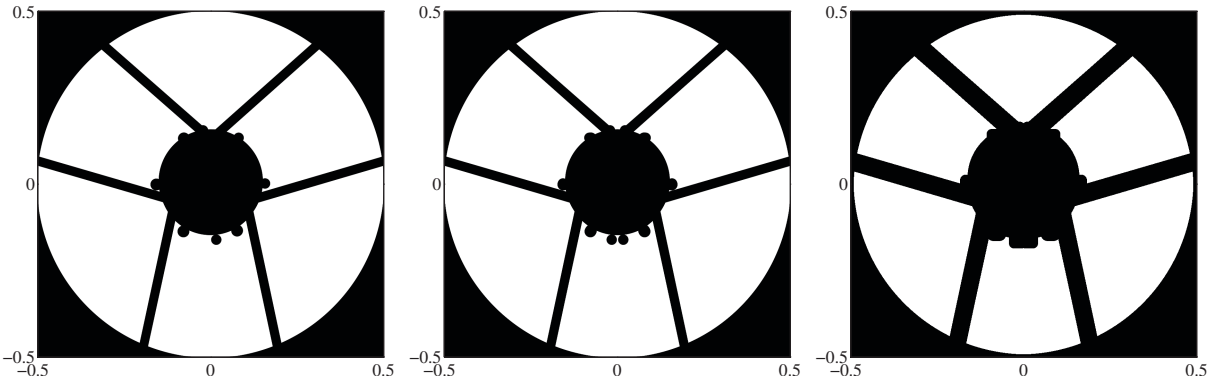

(a) Nominal Pupil (b) Symmetrized Pupil (c) 1%-Padded, Symmetrized Pupil

Figure 1. (a) Nominal AFTA pupil de-rotated to have approximate y-axis symmetry. (b) Nominal AFTA pupil symmetrized about the y-axis for SP optimization. (c) Symmetrized pupil with 10-pixels of padding.

Here we quantitatively analyze the effect of pupil padding on a characterization mask with a fixed OWA of $10\lambda/D$ and search area contrast of 10^{-8}. Results are listed in Table 3.2, where transmission is given as the ratio compared to the nominal, asymmetric pupil. We padded the 1000×1000 symmetrized pupil by up to ten pixels.

For small amounts of padding, the largest loss is in minimum achievable IWA. Any padding at all brings the IWA from $3.4\lambda/D$ to $4.1\lambda/D$. This may be a result of making the edges of the obstructions jagged (discretized). One way to test this idea would be to optimize SPs for anti-aliased AFTA pupils with thicker spiders and see if the IWA is better than for the padded pupil, but we have not yet tested this hypothesis. For larger amounts of padding (> 2 pixels), the only performance degradation is in transmission.

Padded Pixels:	None	0	1	2	3	4	5	6	7	8	9	10
T_{pupil}	.995	.990	.971	.953	.935	.926	.910	.895	.880	.865	.850	.835
T_{SP}	.437	.540	.516	.492	.471	.464	.438	.411	.385	.358	.332	.306
IWA_{min} $(\frac{\lambda}{D})$	3.4	4.1	4.1	4.1	4.2	4.2	4.2	4.2	4.2	4.2	4.2	4.2

Table 1. Characterization masks (60°, 10^{-8} contrast) with a padded pupil for OWA= $10\lambda/D$. Transmission ratios are calculated compared to the nominal pupil, which is why the non-padded pupil transmission is not 100%.

The two major questions when padding the pupil are 1) how much padding is necessary and 2) what happens to performance if the pupil and SP are not aligned? In one optical simulation we performed, the SP performance was very sensitive to misalignment. The 1000x1000 characterization mask with zero-pixels of padding was translated by one pixel in x compared to the actual pupil. Even with wavefront control, the nominal search area reached a floor of 10^{-7} contrast, a full order of magnitude worse than the design level. Some pupil padding is therefore necessary for the AFTA pupil, but the exact amount will depend on the capabilities of the pupil camera and SP mount actuators. Because the SP is reflective, a precision actuation mount is already necessary to steer the beam correctly. In addition, a pupil camera with the same resolution as the SP (1000×1000) is reasonable. We therefore expect that one to three pixels of padding will be enough for AFTA, where a SP pixel in this case is ≈24 microns on a side.

3.3 Shaped Pupils Produced for AFTA

Our specific designs for the characterization and discovery masks have changed once already and will continue to change during pre-Phase A for WFIRST-AFTA as we design for revised pupil geometries, specific observing scenarios, fewer total masks, and greater pupil alignment tolerance. Here we present the shaped pupils that have been simulated, manufactured, and tested in the High Contrast Imaging Testbed at JPL. The characterization mask is shown in Fig. 2 and the discovery mask is shown in Fig. 3. Both have zero pixels of padding, which we will increase in a future iteration. We used the minimum possible IWA for the characterization mask, which was $4.0\lambda/D$ for the other parameters we chose (OWA=$12.5\lambda/D$ and 10^{-8} contrast). The IWA and OWA are better for this mask than that reported in Table 3.2 because a slightly more aggressive padding of gray pixels was used when making the table. The discovery mask has a much larger IWA of $7.0\lambda/D$, so it would have to be used at the bluest observing band to match the same sky angle as the characterization mask in the redder bandpasses for the integral field spectrograph. In a later iteration of the AFTA SP designs, we will most likely switch to a discovery mask with an IWA of about $6\lambda/D$, which then limits the OWA to about $15\lambda/D$. When trying to decrease the IWA of the discovery mask, the maximum possible OWA decreases much faster. This means an IWA below about $6\lambda/D$ is not practical for the discovery mask.

The first set of AFTA SP designs have already been manufactured in JPL's MDL and tested in JPL's HCIT. For the initial tests only a single DM has been available, so only a single-sided dark holes is feasible. Using a reflective characterization SP, the team led by Eric Cady in the HCIT has achieved sub-10^{-8} contrast in the dark hole in monochromatic light, slightly better than the design contrast of the coronagraph. Broadband and double-sided results will be reported in a future publication.

3.4 Performance Degradation Due to Manufacturing Defects

Along with the manufacturing worries in Section 2, we must also consider the effect of overetching or underetching of the SP pixels. Overetching of the black silicon on a reflective mask corresponds to underetching of aluminum on a transmissive, Al-on-glass mask. SP pixels will be roughly 10-30 microns across (assuming 1000 points across and 10-30mm pupil) for most foreseeable applications, and the edges of etched SP pixels can be uniformly off by

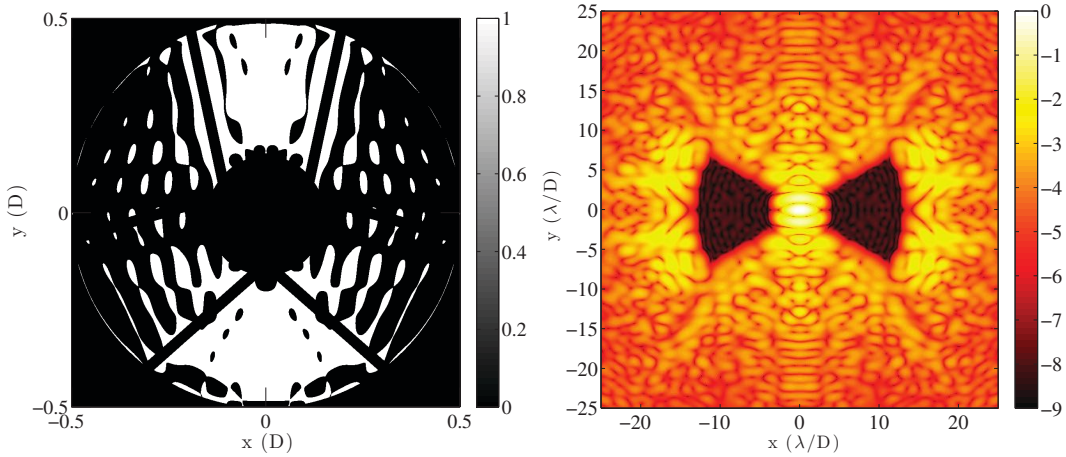

(a) Characterization Mask (b) Ideal PSF of Characterization Mask

Figure 2. (a) Characterization mask for AFTA with IWA=$4.0\lambda/D$, OWA=$12.5\lambda/D$, and pupil transmission of 40%. Scale is linear. (b) Ideal PSF on a log_{10} scale. Average contrast is 1×10^{-8} in the search area.

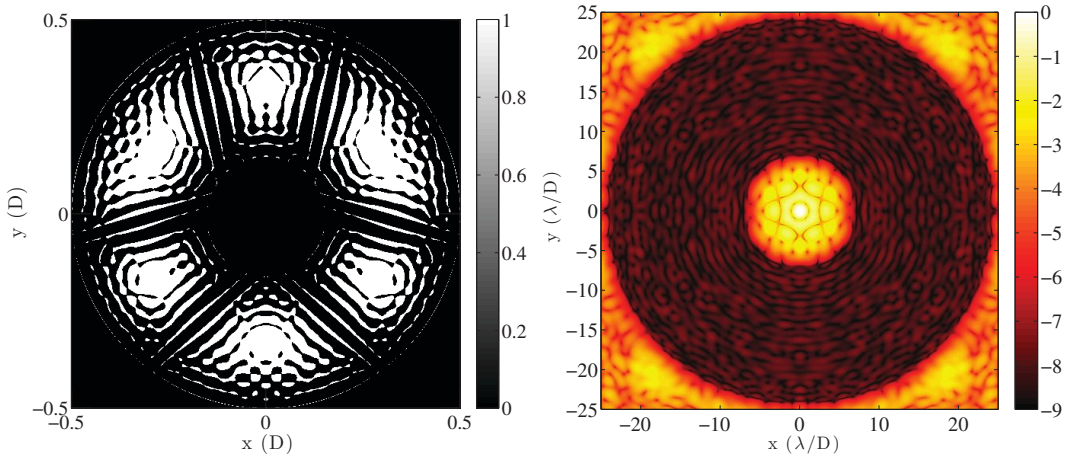

(a) Discovery Mask (b) Ideal PSF of Discovery Mask

Figure 3. (a) Discovery mask for AFTA with IWA=$7.0\lambda/D$, OWA=$24\lambda/D$, and pupil transmission of 37%. Scale is linear. (b) Ideal PSF on a log_{10} scale. Average contrast is 1×10^{-8} in the search area.

a few microns. We therefore need to know how much overetching/underetching tolerance is allowed when trying to achieve a given contrast.

In Table 3.4 we present the results of a quick analysis of the effects of black silicon overetching. We calculate the degradation of the average contrast in the ideal, no-aberration PSF since the degradation appears to be uniform across the search area. In our simple model, we upsample each pixel of the 1000×1000 SP into an $n \times n$ array of pixels of the same transmission (white= 1, black= 0). Then, we loop over all the pixels in this $(n \times 1000) \times (n \times 1000)$ SP and convert to black any white pixel neighboring a black pixel. This simulates an overetch ratio of $1/n$; for example, $n = 16$ corresponds to an overetch of 6.25%. Then, we perform a discrete Fourier transform (DFT) from the SP to the focus before measuring the average contrast in the search area. We expect that wavefront control will be able to recover some of the lost contrast but not very much (maybe a factor of 2 or 3) because etching errors are binary amplitude errors, which are hardest for the DMs to counteract. Other manufacturing errors such as pinholes or stray pieces of dust or metal are hard to model generically and are probably best modeled using the errors found on an actual manufactured mask.

% Overetch	0	5	6.25	10	14.3	20
Avg. Contrast ($\times 10^{-8}$)	0.98	2.0	2.6	5.2	9.6	17.9

Table 2. Contrast degradation values for different amounts of black silicon overetch of the SP design.

4. SHAPED PUPIL LYOT CORONAGRAPHS (SPLC) FOR AFTA

We can improve some aspects of the shaped pupil coronagraph by combining it with a hard-edge stop in the Lyot plane. We call this configuration a shaped pupil Lyot coronagraph, or SPLC. The SPLC is different from an apodized pupil Lyot coronagraph (APLC)[8] because the design method requires no assumption about symmetry in either the pupil or focal plane, whereas the APLC solution uses a focal plane mask with circular symmetry. Carlotti et al.[9] and N'Diaye et al.[10] are also investigating aspects of APLCs and SPLCs in these proceedings.

Starting with a SP designed as before, we propagate the apodized, focused beam through the hard-edge FPM, on to a collimating optic leading to a pupil plane conjugate to the SP. This corresponds to the Lyot plane of a classical coronagraph, where we have the opportunity to apply a mask that rejects on-axis starlight, further deepening the contrast in the final image plane. In our model calculations, we find that by combining our baseline SP with a Lyot stop as simple as an iris matched to the nominal telescope pupil, we improve the final monochromatic focal plane contrast by a factor of three. If we incorporate the FPM and Lyot stop in our AMPL optimization model, we can achieve yet higher contrast as well as a smaller IWA. In this scenario, the optimizer modifies the SP apodization pattern so as to diffract on-axis light outside of the iris. In the example shown in Figure 4, we optimize the SP-apodizer for a fixed bowtie-shaped FPM and a circular iris Lyot mask with diameter 90% of the nominal pupil. The added pupil-masking step inherent to the SPLC design breaks the achromatic virtue of the canonical shaped pupil PSF. Currently, we address this chromatic PSF morphology by constraining performance at three wavelengths spanning the desired operating band.

With smaller IWA comes greater sensitivity to aberrations. Our initial simulations show that the SPLC contrast degrades negligibly for the pointing errors one should expect on WFIRST-AFTA and other future space telescopes for direct imaging. The other main error to check is alignment sensitivity. For a characterization FPM, often called a "bow-tie" mask, we must worry about rotational as well as translational alignment. In future work we will investigate the sensitivity of SPLCs to mask alignment errors and more low-order aberrations.

Thus far we have focused on SPLC designs for WFIRST-AFTA. As with the SPs described earlier, we propose using separate characterization masks and discovery masks. Most of the known exoplanets (from radial-velocity detections) on which WFIRST-AFTA is supposed to perform follow-up imaging are at separations less than $4\lambda/D$. Therefore, our primary goal with the SPLC is to reduce the IWA, and our second goal is to improve the contrast. Thus far, we have created designs that achieve sub-10^{-8} contrast in symmetric 70° wedges from 3 to $12.5\lambda_0/D$ in a 10% bandpass, as in Figure 4. The bandwidth can be increased further at the expense of throughput.

5. COMBINED DEFORMABLE MIRROR AND SHAPED PUPIL OPTIMIZATION

This section continues our work reported last year in Carlotti et al.[11] In this section, however, we focus only on optimizing parameters that we can directly control–the stroke of DM actuators and the binary apodization of a shaped pupil. Here we show one way to combine these two sets of parameters in a two-step optimization to achieve high contrast in monochromatic light.

5.1 A Single DM as a Standalone Coronagraph

Many different researchers have realized that phase control in the pupil (or anywhere in the collimated beam) can be used to improve the PSF. Phase-Induced Amplitude Apodization (PIAA) uses two heavily aspheric mirrors or lenses to apodize the outer diameter of the pupil.[12] PIAA is very sensitive to misalignment, however, and requires DMs to mitigate chromatic ringing from the edges of the mirrors. An apodized phase plate (APP) uses a fixed, transmissive optic at the pupil to change the phase and create moderately high contrast on one side of the image plane.[13–15]

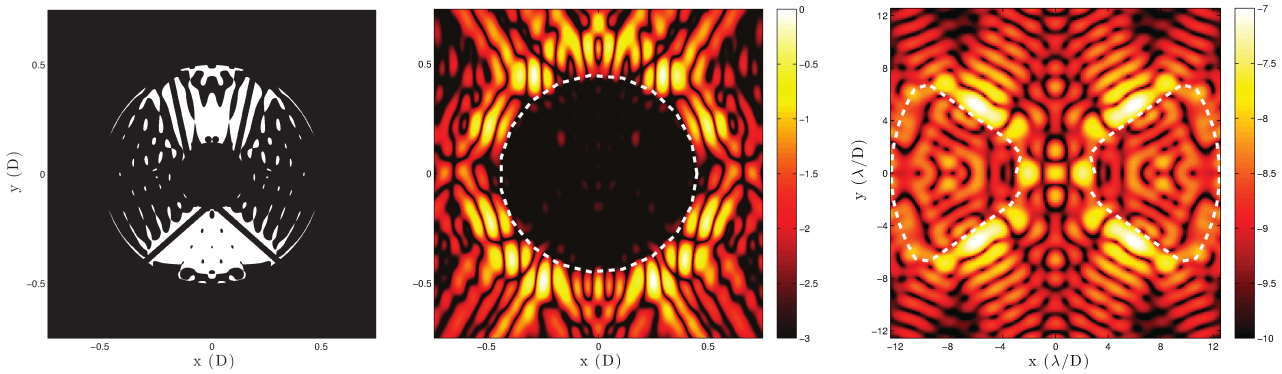

(a) Shaped pupil mask for a SPLC (b) Lyot plane intensity (c) SPLC PSF in final focal plane

Figure 4. (a) Characterization SPLC mask with IWA=3.0λ/D, OWA=12.5λ/D, and 10% bandwidth. (b) Peak-normalized Lyot plane intensity on a log_{10} scale. The dashed line traces the undersized (90 % of nominal diameter) iris acting as the Lyot stop. (c) Monochromatic, zero-wavefront-error PSF at the focus after the Lyot stop, displayed in log_{10} contrast units. The dashed line traces the bowtie-shaped mask used in both the first and second focal planes.

Here we notice that a single DM can also control both amplitude and phase on a single side of the image plane[16] and can thus take the place of an APP. DMs are normally thought of as phase correction devices, but they can also be used for phase control to dig below the nominal PSF of an instrument, coronagraph or not. Therefore, a DM can be used instead of an APP. By running wavefront control (stroke minimization[17] in this case) on the nominal pupil alone, we were able to dig dark holes in the nominal PSF of a telescope down to about 10^{-5} contrast over a 10% bandpass. An example case for the AFTA pupil is shown in Figure 5. In monochromatic light for some pupils and search areas we reached 10^{-6} contrast. The higher the actuator density on the DM, the higher the possible contrast and OWA. Also, because a DM can mitigate some diffractive effects, the DM does not need to be at an actual pupil to be used in place of an APP. This eliminates a set of re-imaging optics and allows the DM simply to take the place of a fold mirror somewhere near the pupil. In addition, when switching from one bandpass to another one simply has to scale the actuator heights on the DM instead of switching plates. The APP may be able to achieve a slightly better IWA than our optimized DM surface because a DM cannot actuate as many modes as can be included in an APP. The peak-to-valley stroke required on the DM increases for higher contrast and has a maximum of about a wave. These actuation heights may be small enough to be the static starting position of DMs already part of an observatory. This method of optimization differs from that described in Pueyo et al.,[18,19] in which they use Active Compensation of Aperture Discontinuities (ACAD) with two DMs to apodize struts and primary mirror segment gaps. ACAD conserves path length and optimizes nonlinearly in the pupil plane whereas our optimization does not conserve path length (since only one DM is used) and uses a linear optimization.

5.2 Hybrid One-DM and Shaped Pupil Coronagraph

As the input for the second stage of the two-step 1DM+SP coronagraph, we used the phase map created in the previous section via broadband stroke minimization. To speed up the SP part of the optimization, we utilized a zero-padded, y-axis symmetrized AFTA pupil as the input pupil for the first step. This yielded a DM surface optimization with an antisymmetric profile about the y-axis. As explained with phasors in Pueyo et al.,[17] the DM is moving amplitude from one side of the image plane to the other. In the second step of the 1DM+SP coronagraph optimization, we optimize a SP using the symmetrized AFTA pupil and the antisymmetric phase map as the starting point. From running SP optimizations over the full pupil (for a one-sided search area), we found that the SP optimization yields a mask symmetric about the y-axis, which is not an obvious result. Knowing that the phase is antisymmetric and that the SP will be symmetric about the y-axis, we can now develop a faster optimization model for input into AMPL.

Our goal is to exploit the symmetries of the problem in order to make it more tractable. We look at the double integral for the Fourier transform that defines the focal plane electric field, $E_{foc}(\xi, \eta)$. We use normalized

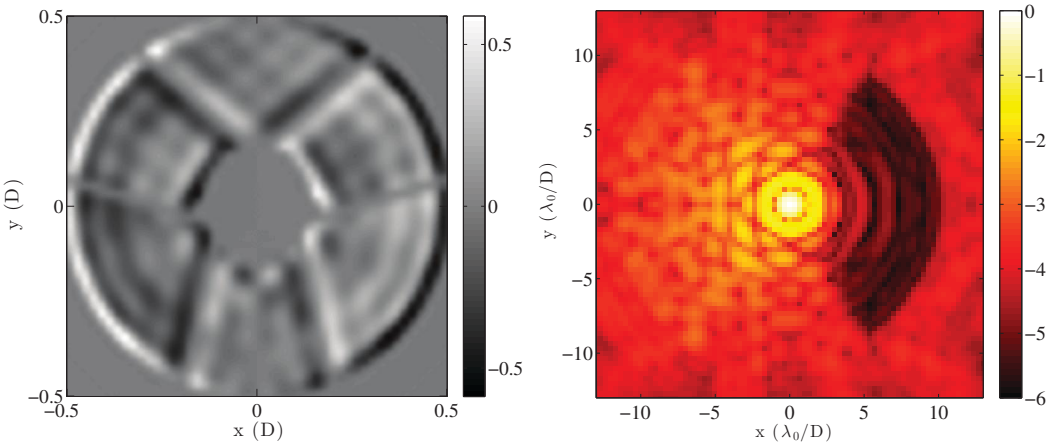

(a) DM Surface (b) Resulting PSF

Figure 5. (a) Actuated DM surface in units of waves from a 48x48 DM. (b) Ideal 10%-broadband PSF on a log_{10} scale of the actuated DM conjugate to the symmetrized AFTA pupil. Average contrast is 2×10^{-5} between radii of 3 and $12\lambda_0/D$ over a 120° arc.

units such that (x, y) are in units of pupil diameter D and (ξ, η) are in units of λ/D. Following Vanderbei's original 2-D SP optimization,[2] we group the double integral into an inner integral over x, denoted as $\mathcal{C}(\xi, y)$, and an outer one over y,

$$\begin{aligned} E_{foc}(\xi,\eta) &= \mathcal{F}\{A(x,y)e^{i\phi(x,y)}\} \\ &= \iint_{-1/2}^{1/2} A(x,y)e^{i\phi(x,y)}e^{-i2\pi(x\xi+y\eta)}dxdy \\ &= \int_{-1/2}^{1/2}\left(\int_{-1/2}^{1/2} A(x,y)e^{i\phi(x,y)}e^{-i2\pi x\xi}dx\right)e^{-i2\pi y\eta}dy \\ &= \int_{-1/2}^{1/2} \mathcal{C}(\xi,y)e^{-i2\pi y\eta}dy, \end{aligned} \tag{1}$$

where $\phi(x, y)$ is DM surface conjugate to a pupil, $A(x, y)$ is the pupil electric field, and $\mathcal{F}\{\cdot\}$ is the Fourier transform. As with an FFT, this two-stage integral makes tractable large problems that would be impossible to solve with a brute-force 2-D Fourier transform. On a computer all these integrals become discrete summations over x and y, but in this derivation we leave the integral notation for convenience. To exploit the symmetries about the y-axis, we split $\mathcal{C}(\xi, y)$ into the sum of two integrals, one over $x \in [-1/2, 0]$ and the other over $x \in [0, 1/2]$. Recall that $A(x, y) = A(-x, y)$ from symmetry and that $\phi(x, y) = -\phi(-x, y)$ from antisymmetry. If we define $x' = -x$ (and thus $dx' = -dx$), we find

$$
\begin{aligned}
\mathcal{C}(\xi, y) &= \int_{-1/2}^{0} A(x,y) e^{i\phi(x,y)} e^{-i2\pi x\xi} dx + \int_{0}^{1/2} A(x,y) e^{i\phi(x,y)} e^{-i2\pi x\xi} dx \\
&= \int_{1/2}^{0} A(x',y) e^{-i\phi(x',y)} e^{i2\pi x'\xi} (-dx') + \int_{0}^{1/2} A(x,y) e^{i\phi(x,y)} e^{-i2\pi x\xi} dx \\
&= \int_{0}^{1/2} A(x',y) e^{-i\left(\phi(x',y) - 2\pi x'\xi\right)} dx' + \int_{0}^{1/2} A(x,y) e^{i(\phi(x,y) - 2\pi x\xi)} dx \\
&= \int_{0}^{1/2} A(x,y) \left(e^{-i(\phi(x,y) - 2\pi x\xi)} + e^{i(\phi(x,y) - 2\pi x\xi)} \right) dx \\
&= 2 \int_{0}^{1/2} A(x,y) \cos\left(\phi(x,y) - 2\pi x\xi\right) dx, \qquad (2)
\end{aligned}
$$

which is a purely real result.

The last step is to calculate $E_{foc}(\xi, \eta)$. Since the AFTA pupil has no x-axis symmetry, $E_{foc}(\xi, \eta)$ will have both real and imaginary parts. AMPL does not allow complex numbers, so we will derive the expressions for the real part, denoted by $Re\{\}$, and imaginary part, denoted by $Im\{\}$, separately as

$$
\begin{aligned}
Re\{E_{foc}(\xi,\eta)\} &= \int_{-1/2}^{1/2} \mathcal{C}(\xi, y) \cos(2\pi y\eta)\, dy \\
Im\{E_{foc}(\xi,\eta)\} &= -\int_{1/2}^{1/2} \mathcal{C}(\xi, y) \sin(2\pi y\eta)\, dy \qquad (3)
\end{aligned}
$$

Now that we have the physics of the problem to include as linear constraints, we need to finish defining our linear program. Our objective function in the SP optimization is the transmission of the pupil, which is just a double sum over $A(x, y)$. We choose to maximize the transmission because we want to utilize as much light as possible from faint exoplanets. The last constraint we want is on the contrast in the search area. Even though the contrast is quadratic because the intensity is the square of the electric field, we can use linear constraints for nearly the same effect. (We are constraining the real and imaginary part of the electric field to the box bounded by the square root of the contrast times $\pm 1/\sqrt{2}$ and $\pm i/\sqrt{2}$ in the real-imaginary plane, whereas we would prefer the slightly less strict bound of the unit circle times the square root of the contrast.) We want the absolute value of the electric field in the search area to be less than or equal to the square root of the desired contrast, $c = 8$ in this case, so our linear constraints on contrast are

$$
\begin{aligned}
-10^{-c/2} E(0,0)/\sqrt{2} \le Re\{[E_{foc}(\xi,\eta)]_{SearchArea}\} \le 10^{-c/2} E(0,0)/\sqrt{2} \\
-10^{-c/2} E(0,0)/\sqrt{2} \le Im\{[E_{foc}(\xi,\eta)]_{SearchArea}\} \le 10^{-c/2} E(0,0)/\sqrt{2}, \qquad (4)
\end{aligned}
$$

where $E(0,0) = Re\{E(0,0)\}$ because, as we can see in Eq. 3, the imaginary part of the focal plane electric field is an odd function and thus zero at the core.

In figure 6 we show one example of a 1DM+SP coronagraph. The search area is at 10^{-8} contrast from 4 to 10 λ/D over a 60° arc. To make up for added complexity compared to a standalone SP, the 1DM+SP needs to

have some benefit. We can usually obtain higher pupil mask transmission than with a SP alone, and sometimes we can get a better IWA. The loss of one side of the dark hole by using a DM would not matter when imaging an exoplanet because it would be located on just one side of the star anyway. If a dark hole were needed on the other side of the star, the negative of those DM commands would change the dark hole location accordingly.

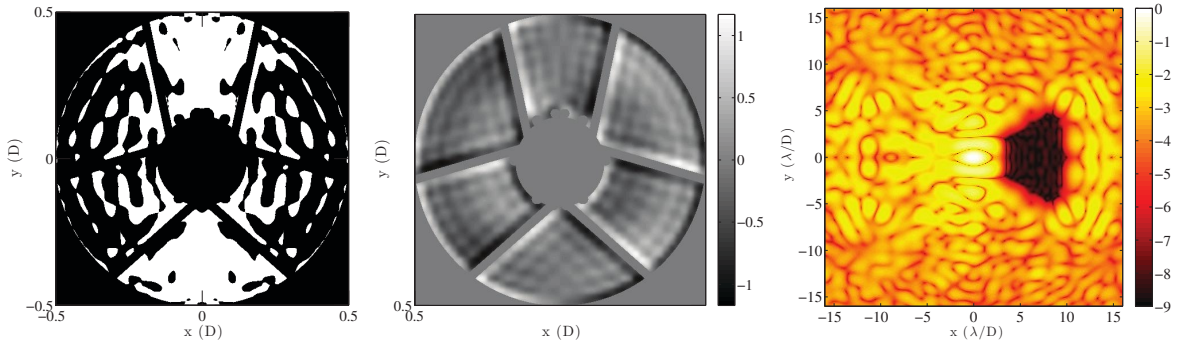

(a) SP (b) Phase from DM (Units = λ) (c) PSF from 1DM+SP

Figure 6. An example of a symmetric SP combined with an antisymmetric DM surface to create a one-sided search area.

The largest problem is chromaticity of the solution. If a monochromatic 1DM+SP for 10^{-8} contrast sees a 10% bandpass, the average broadband contrast degrades to about 10^{-6}. If the SP mask is designed with a given DM surface for a 10% bandpass, the pupil mask transmission ends up on the order of 1%. In addition, these antisymmetric designs may be very sensitive to dead actuators, DM clocking, or DM translation. Therefore, a DM may not be practical for providing the phase in this type of coronagraph design.

Instead, we propose combining a shaped pupil with a vector apodized phase plate as presented in Otten et al.[20] By utilizing dielectrics to counter chromaticity, they were able to manufacture broadband, transmissive phase plates based on monochromatic phase optimizations as described by Codona.[13,21] Metal-on-glass binary apodizers already exist,[5] so it should be simple to include an aluminum or chrome SP underneath the vector APP dielectrics or on the other side of the glass plate to create a Shaped Pupil Phase Plate (SPPP). This SPPP would have a higher throughput than a SP alone and would achieve a higher contrast than an APP could alone. As with any multi-step optimization procedure, we are still investigating the behavior of certain classes of solutions for the SPPP.

Through our 1DM+SP optimization procedure, we have also discovered an easy way to design APPs. We can use stroke minimization on an arbitrary pupil to obtain a DM surface and then make that phase map with an APP. Since we are not using a real DM anymore, we can also increase the number of actuators on this pretend DM to control higher spatial frequencies with the APP.

6. SHAPED PUPIL DESIGN FOR EXO-C

While the SP was chosen for the AFTA coronagraph, it was not selected for the Exo-C probe mission study.[22] Exo-C would have an unobstructed circular pupil and better pointing stability than AFTA. That combination meant that the other coronagraphs (hybrid Lyot, vector vortex, and PIAA) would achieve better IWA, throughput, and contrast levels than a SP. Figure 7 shows the SP considered for Exo-C. It has a raw contrast of 10^{-9} from 3.4 to 24.0λ/D with a pupil transmission of 20.8%. For a raw contrast of 10^{-10} in the same region, the IWA would rise to 3.8λ/D.

For an unobscured aperture, we found that the trick of using separate characterization and discovery masks did not work. With 60° search area openings, the best IWA we could achieve was 3.0λ/D at 1×10^{-9} contrast. We deemed this small improvement in IWA as too small to justify imaging two 60° openings over the full 360° region around the star. From the SP design in this paper, it seems that a characterization mask IWA is limited to $\approx 3 - 4\lambda/D$ at high contrast no matter what the initial pupil is. A characterization mask is only helpful for an obscured aperture, in which case the IWA of a 360° search area mask is much larger than for an unobscured pupil.

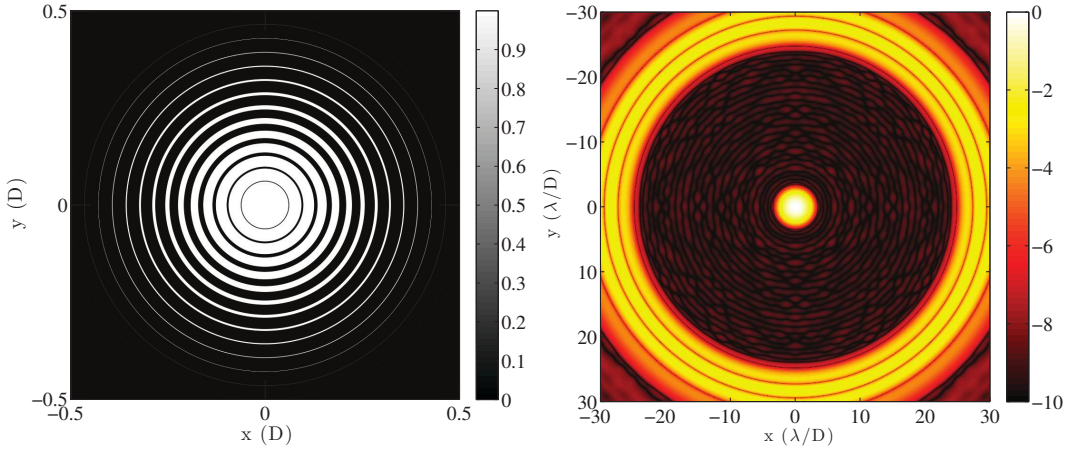

(a) Concentric Ring SP (b) PSF from Ring SP

Figure 7. (a) Concentric ring shaped pupil, shown on a linear scale, for the Exo-C study. Pupil transmission is 20.8%. (b) Ideal PSF from the ring mask on a log_{10} scale. Average contrast is 1×10^{-9} between radii of 3.4 and $24\lambda/D$.

7. CONCLUSIONS

Shaped pupils are a good match to the challenging AFTA pupil and were selected for the WFIRST-AFTA coronagraph instrument. Our 2-D optimized, non-freestanding SP designs are finally realizable with the reflective shaped pupil manufacturing process, which uses black silicon for absorptive regions and aluminum for reflective areas, invented at JPL's MDL. The first reflective SP experiment performed this spring with one DM and monochromatic light in JPL's HCIT shows that the SP performs to specifications. This result, which was achieved within days of installing the SP in the testbed, demonstrates the simplicity and robustness of SPs for high contrast imaging with WFIRST-AFTA.

To increase the performance of an SP even further, we can add a Lyot stop or utilize phase at the pupil plane. A SPLC utilizes a Lyot stop to obtain better contrast and/or IWA than a SP alone with a slight increase in sensitivity to chromaticity and low-order aberrations. We are investigating SPLC designs that would improve the science yield for AFTA with the given constraints to pointing and available observation time. Combining an APP with a SP is another possible way to increase throughput and improve IWA compared to a SP alone, but this technology is premature for the AFTA coronagraph. In the meantime, we will continue to develop better SP and SPLC designs for AFTA that account for realistic errors and aberrations.

Acknowledgements

This work was funded by NASA Technology Development for Exoplanet Missions (TDEM) grant #NNX09AB96G and NASA Astrophysics Research and Analysis (APRA) grant #NNX12A151G.

REFERENCES

[1] Carlotti, A., Vanderbei, R., and Kasdin, N., "Optimal pupil apodizations of arbitrary apertures for high-contrast imaging," *Optics Express* **19**(27), 26796–26809 (2011).

[2] Vanderbei, R., "Fast fourier optimization, sparsity matters," *Mathematical Programming Computation* , 1–17 (2012).

[3] Belikov, R., Give'on, A., Kern, B., Cady, E., Carr, M., Shaklan, S., Balasubramanian, K., White, V., Echternach, P., Dickie, M., Trauger, J., Kuhnert, A., and Kasdin, N. J., "Demonstration of high contrast in 10% broadband light with the shaped pupil coronagraph," *Proceedings of SPIE* **6693**, pp. 66930Y–1 – 66930Y–11 (Sept. 2007).

[4] Balasubramanian, K., Wilson, D., White, V., Muller, R., Dickie, M., Ruiz, R., Shaklan, S., Cady, E., Kern, B., Belikov, R., Guyon, O., and Kasdin, N., "High contrast internal and external coronagraph masks produced by various techniques," in [*Proceedings of SPIE*], **8864**, 88641R (2013).

[5] Martinez, P., Dorrer, C., Carpentier, E. A., Kasper, M., Boccaletti, A., Dohlen, K., and Yaitskova, N., "Design, analysis, and testing of a microdot apodizer for the apodized pupil lyot coronagraph," *Astronomy and Astrophysics* **495**, 363–370 (2009).

[6] Soummer, R., Sivaramakrishnan, A., Oppenheimer, B., Roberts, R., Brenner, D., Carlotti, A., Pueyo, L., Macintosh, B., Bauman, B., Palmer, D., et al., "The gemini planet imager coronagraph testbed," in [*Proceedings of SPIE*], **7440**, 74400R (2009).

[7] Carlotti, A., Kasdin, N. J., and Vanderbei, R. J., "Shaped pupil coronagraphy with wfirst-afta," in [*Proceedings of SPIE*], **8864**, 886410 (2013).

[8] Soummer, R., "Apodized pupil lyot coronagraphs for arbitrary telescope apertures," *The Astrophysical Journal Letters* **618**(2), L161 (2005).

[9] Carlotti, A., Pueyo, L., Mawet, D., and N'Diaye, M., "Three possible types of apodized coronagraphs for the E-ELT PCS instrument," in [*Proceedings of SPIE*], **9147** (2014).

[10] N'Diaye, M., Pueyo, L., Soummer, R., Carlotti, A., Choquet, E., and Perrin, M., "Apodized pupil Lyot coronagraphs: numerical optimization of apodizer transmission with psf dark zone," in [*Proceedings of SPIE*], **9143** (2014).

[11] Carlotti, A., Kasdin, N. J., Vanderbei, R. J., and Riggs, A., "Hybrid coronagraphic design: optimization of complex apodizers," in [*Proceedings of SPIE*], **8864**, 88641Q (2013).

[12] Guyon, O., "Phase-induced amplitude apodization of telescope pupils for extrasolar terrestrial planet imaging," *Astron. Astrophys* **404**, 379 (2003).

[13] Codona, J. L., Kenworthy, M. A., Hinz, P. M., Angela, J., and Woolf, N., "A high-contrast coronagraph for the MMT using phase apodization: design and observations at 5 microns and 2 lambda/d radius," in [*Proceedings of SPIE*], **6269**, 62691N (2006).

[14] Codona, J., "Phase apodization coronagraphy," in [*In the Spirit of Bernard Lyot: The Direct Detection of Planets and Circumstellar Disks in the 21st Century*], **24** (2007).

[15] Kenworthy, M. A., Quanz, S. P., Meyer, M. R., Kasper, M. E., Lenzen, R., and Codona, J. L., "An apodizing phase plate coronagraph for VLT/NACO," in [*Proc. SPIE*], **7735** (2010).

[16] Shaklan, S. B. and Green, J. J., "Reflectivity and optical surface height requirements in a broadband coronagraph. 1.Contrast floor due to controllable spatial frequencies," *Applied Optics* **45**, 5143–5153 (July 2006).

[17] Pueyo, L., Kay, J., Kasdin, N., Groff, T., McElwain, M., Give'on, A., and Belikov, R., "Optimal dark hole generation via two deformable mirrors with stroke minimization," *Applied Optics* **48**(32), 6296–6312 (2009).

[18] Pueyo, L. and Norman, C., "High-contrast imaging with an arbitrary aperture: Active compensation of aperture discontinuities," *Astrophysical Journal* **769**(102) (2013).

[19] Pueyo, L., Norman, C., Soummer, R., Perrin, M., N'Diaye, M., and Choquet, E., "High contrast imaging with an arbitrary aperture: Active correction of aperture discontinuities," in [*Proceedings of SPIE*], **8864**, 88640Z (2013).

[20] Otten, G., Snik, F., Kenworthy, M. A., Codona, J., Escuti, M., and Miskiewicz, M. N., "The vector apodizing phase plate coronagraph: prototyping and new developments," in [*Proceedings of SPIE*], **9151** (2014).

[21] Codona, J. L. and Angel, R., "Imaging extrasolar planets by stellar halo suppression in separately corrected color bands," *Astrophysical Journal* **604**, L117–L120 (2004).

[22] Stapelfeldt, K., Belikov, R., Bryden, G., Cahoy, K., Chakrabarti, S., Marley, M., McElwain, M., Meadows, V., Serabyn, E., and Trauger, J., "Exo-C: Imaging nearby worlds interim report," tech. rep., NASA (2014).